HAIT Journal of Science and Engineering B, Volume 2, Issues 5-6, pp. 787-807

Novel improvements for matrix converter fed adjustable speed drive system

Yang Mei*, Kai Sun, Daning Zhou, Lipei Huang, and Xuansan Cai

Department of Electrical Engineering,
Tsinghua University, Beijing, China
Corresponding author: meiy03@mails.tsinghua.edu.cn

Received 1 March 2005, accepted 23 June 2005

Abstract

Matrix converter (MC) is a direct energy conversion device with high input power factor and regeneration capability. As a device without dc link elements, it possesses a series of properties different from traditional AC-DC-AC converters, which are the objects of research. In this paper, a novel power device application and high performance control for a matrix converter fed induction motor drive system, as well as the behavior the MC drive under abnormal input voltage conditions, have been investigated. A 3-3 MC prototype using the newly developed IGBT with reverse blocking capability (RB-IGBT) is constructed; a control strategy to combine space vector modulation and vector control technique for matrix converter fed induction motor drive system is proposed; two compensation methods are proposed to improve the output performance of MC and ensure the drive performance of induction motor under abnormal input voltage conditions. The effectiveness and feasibility of the proposed improvement have been proven through numerical simulations and experimental tests.

Keywords: Electronics, power circuits, communication circuits, simulation, switches

1 Introduction

The matrix converter (MC) is a direct power conversion device that generates variable magnitude and variable frequency output voltage from the ac

utility grid. It creates sinusoidal currents with unity power factor and fully regeneration capability. Since it does not involve a dc voltage link and associated large capacitor, a MC drive has higher power density than a PWM inverter drive [1-3].

During recent years, the MC technology has entered the power electronics industry but only a few of practical matrix converters have been designed. The primary obstacle is that there is no individual device available to serve as the bi-directional power switch which is a basic cell of MC. In this paper it will be shown that a newly developed IGBT with reverse blocking capability (RB-IGBT) helps to realize the essential element with low power losses. A 3-3 MC prototype using the RB-IGBT is constructed, and a three-stage driving method and novel protection circuit for RB-IGBT are designed and implemented.

In order to realize high performance control of matrix converter fed induction motor drive system, a control strategy, which combines both space vector modulation and direct field oriented control, is proposed in this paper. Space vector modulation is employed to regulate the input/output sinusoidal waveforms of matrix converter with unity input power factor. The direct field oriented control technique based on adaptive flux observer is applied to ensure a good drive performance of induction motor. The proposed control strategy is implemented by a combined controller, which combines advantages of the MC with advantages of the vector control technique.

Since the MC is a direct frequency conversion device, the disturbances at the input grid side, such as unbalance and short-time voltage sag, are immediately reflected to the load side, deteriorating the drive performance of induction motors. This paper also proposed a feed-forward compensation method to compensate the output waveforms. Experimental tests have been carried out on a 2.7kW prototype of MC fed induction motor drive system.

2 New power device application for matrix converter

2.1 Introduction of MC

A three-phase to three-phase MC consists of nine bi-directional switches to connect the input phases a, b, c to the output phases A, B, C as it is shown in Fig. 1.

Each of these bi-directional switches can be constructed by power semiconductor devices as shown in Fig. 2. Traditionally, two IGBTs with

anti-paralleled diodes are connected in series to construct one bi-directional switch (Fig. 2a). However, this structure requires 18 IGBTs and 18 diodes, resulting in much more power loss than in conventional AC-DC-AC converters and hindering the further popularization of the MC.

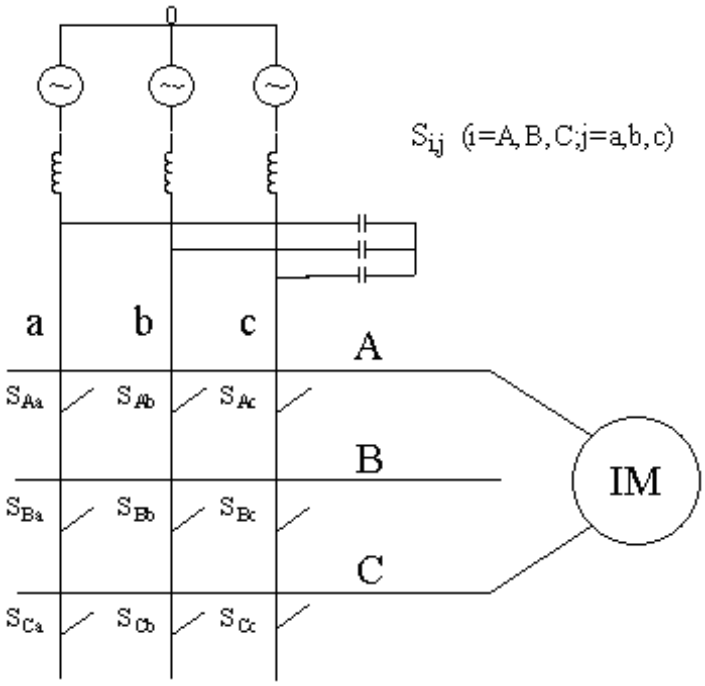

Figure 1: The topology of three-phase to three-phase matrix converter.

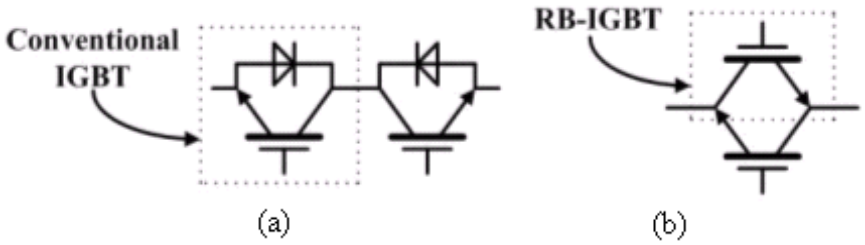

Figure 2: Different structures of bi-directional power switches: (a) conventional IGBTs with diodes; (b) RB-IGBTs.

Newly developed IGBT with reverse blocking capability (RB-IGBT) helps to resolve this problem. A bi-directional switch is realized by a simple placing of two RB-IGBTs in anti-parallel while 18 diodes used for blocking the voltage in matrix converter are no longer required (Fig. 2b).

The most general MC modulation strategy is the indirect modulation, which decouples the control of the input current and the output voltage and regards the matrix converter as a cascade connection of two stages, a voltage source rectifier and a voltage source inverter (shown in Fig. 3). Using this connection, the conventional space vector modulation technique can be applied to the rectifier and inverter stage, respectively [3].

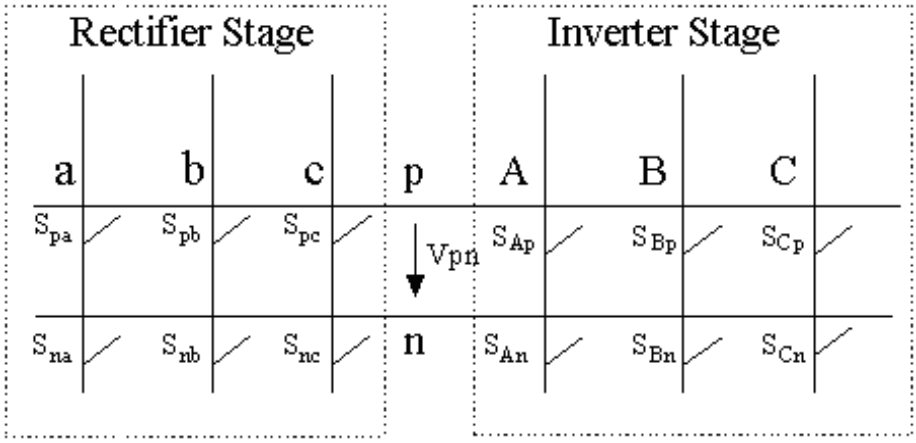

Figure 3: The indirect modulation model of matrix converter.

Fig. 4a shows the input current switching vector hexagon where $\vec{V_i}$ is the input phase voltage space vector and φ_i is the input displacement angle. As shown in Fig. 4b, the reference input phase current space vector $\vec{I_i^*}$ is generated by impressing the adjacent switching vector $\vec{i}_\mu$ and $\vec{i}_\nu$ to regulate the input currents as sinusoidal waveforms. The input power factor is controllable through the setting input displacement angle φ_i. The duty cycles d_μ and d_ν of $\vec{i}_\mu$ and $\vec{i}_\nu$ are calculated as

$$d_\mu = m_c \sin(\frac{\pi}{3} - \theta_{sc}) \tag{1}$$

$$d_\nu = m_c \sin(\theta_{sc}) \tag{2}$$

where $m_c = 1$ is the current modulation index.

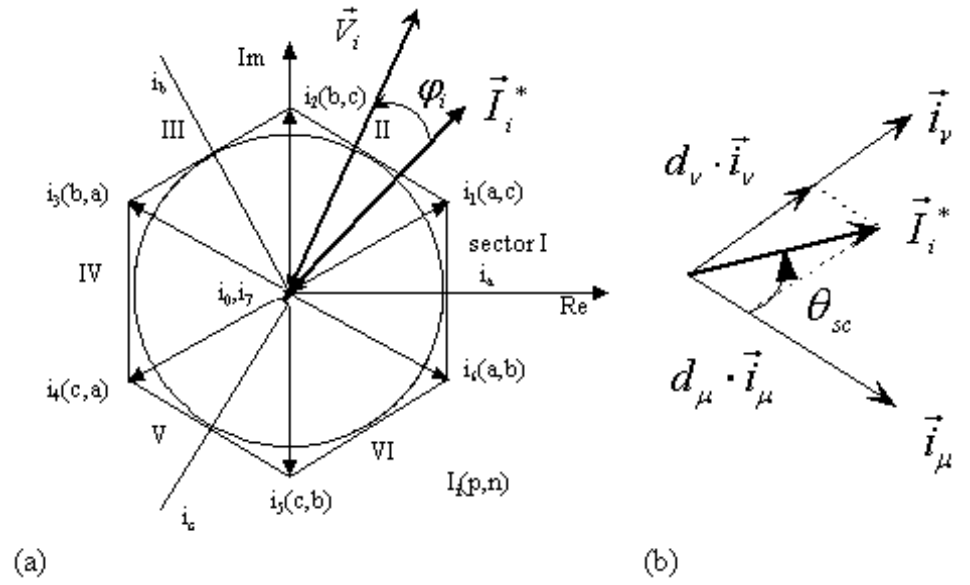

Figure 4: (a) Input current switching vector hexagon. (b) Generation of the reference input curent space vector.

Similarly, Fig. 5a shows the output voltage switching vector hexagon. As shown in Fig. 5b, the reference output line voltage space vector $\vec{V}_o^*$ is generated by impressing the adjacent switching vector $\vec{V}_\alpha$ and $\vec{V}_\beta$ to regulate the output voltages as sinusoidal waveforms. The duty cycles $d_\alpha$and d_β of $\vec{V}_\alpha$and $\vec{V}_\beta$ are calculated as

$$d_\alpha = m_v \sin(\frac{\pi}{3} - \theta_{sv}) \tag{3}$$

$$d_\beta = m_v \sin(\theta_{sv}) \tag{4}$$

where m_v is the voltage modulation index.

The entire modulation of MC is established by the combination of two space vector modulation strategies. The switching pattern for the entire converter is generated by a product of the corresponding duty cycles:

$$\begin{array}{ll} d_{\alpha\mu} = d_\alpha \cdot d_\mu, & d_{\beta\mu} = d_\beta \cdot d_\mu \\ d_{\beta\nu} = d_\beta \cdot d_\nu, & d_{\alpha\nu} = d_\alpha \cdot d_\nu \end{array} \tag{5}$$

$$d_0 = 1 - (d_{\alpha\mu} + d_{\beta\mu} + d_{\beta\nu} + d_{\alpha\nu}). \tag{6}$$

The duration of each switching sequence, such as $\alpha\mu$, $\beta\mu$, $\beta\nu$, $\alpha\nu$, is calculated by multiplying the corresponding duty cycle by one sampling period T_s, and distributed into switching control signals to drive bi-directional switches.

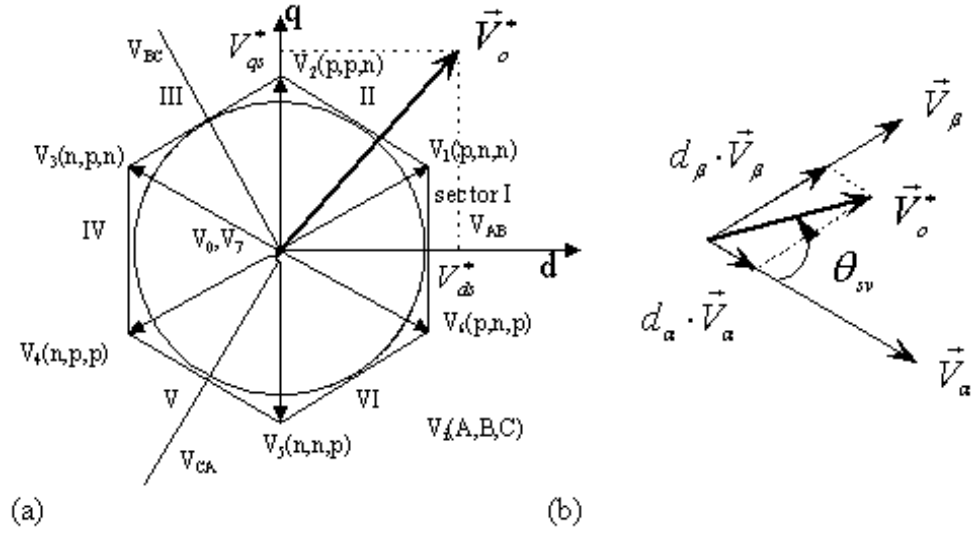

Figure 5: (a) Output voltage switching vector hexagon. (b) Generation of the reference output voltage space vector.

2.2 Three-stage driving and protection circuit for RB-IGBT

Although the voltage-controlled device IGBT is easier to drive than current-controlled devices, much research has been carried out to achieve its better performance [4-6]. In order to reduce the switching power loss, a reduction of the turn-on and turn-off transition is required. However, the increased switching speed results in the increase of turn-on di/dt and turn-off dv/dt. Large electromagnetic interference (EMI) is generated due to the high di/dt and also the IGBT is more probable to be dynamically latched by the increased dv/dt [4]. This conflict is more conspicuous in RB-IGBT which contains no fast recovery diode. During the switching transition of RB-IGBT, the rising slope of collector current and collector-to-emitter voltage is relatively larger than that of the conventional IGBT with anti-paralleled diode [7,8].

According to the gate-charge curve of the device, the turn-on and turn-off transients can be divided into several stages [4]. In the IGBT turn-on transient, the gate charge current can be controlled dynamically. This means that during the rising time of the collector current, the gate charge current is restricted to prevent the increase of di/dt. However, during the time except for collector current rise the gate charge current is enhanced to shorten the transient. Thereby the entire switching transition can be reduced. The shortened collector-to-emitter voltage tail will result in a substantial reduction of the turn-on power loss. In the IGBT turn-off transient similar stages also appear [9].

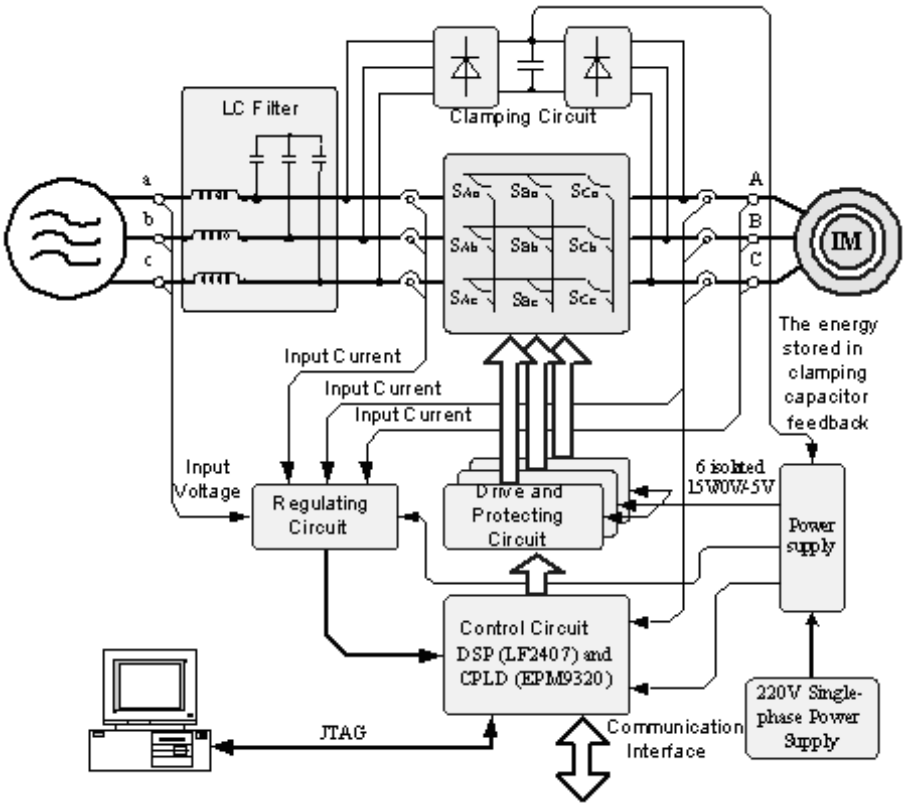

Figure 6: Block diagram of experimental prototype.

Contrary to the common IGBT, in AC-AC conversion RB-IGBT is frequently operated in reverse voltage blocking conditions. Therefore, v_{ce} of RB-IGBT will drop to a negative value. If a traditional protection circuit is employed, the negative voltage will be imported to the driving circuit, leading to the damage of the driver, or even the failure of the whole system.

To resolve this problem, a novel v_{ce} sensing method for RB-IGBT is proposed. By applying a large resistor, v_{ce} of the RB-IGBT is imported into the circuit. Two common diodes or two Zener diodes are used to clamp the v_{ce} within the range of power supply of the driver. A high speed analogue amplifier is applied to increase the detecting precision. A short dead time is also set to avoid switching transition noise. Through the comparison between the amplified v_{ce} and two protection thresholds (applicable in our 600V/100A device), different protection schemes are performed.

2.3 Experimental results

In order to verify advantages of the new power device and the novel detecting method, an experimental prototype of MC fed induction motor drive system has been implemented. The block diagram of the prototype is shown in Fig. 6.

A second-order LC filter is inserted at the input side of the MC. It consists of three series-connected inductors (3 mH) and three star-connected capacitors (5 μF). The clamp circuit is composed of two three-phase rectifiers and a clamp capacitor. The power stage is realized by use of three 600V/100A RB-IGBT 6-1 modules. The parameters of the induction motor are listed in Table 1.

The experiment results are shown in Fig. 7. The sampling frequency is 10kHz, the output frequency is 50Hz, and the motor operates without a load. In Fig. 7a, b, d the current is 1.875 A/div. The input voltages are balanced sinusoidal voltages.

Rating Power 5Hp	Pole Number 2	Rating Frequence 50Hz
Rating Speed 1440 r/m	Rating Current 8.3A	Max Voltage 380V

Table 1. Parameters of induction motor.

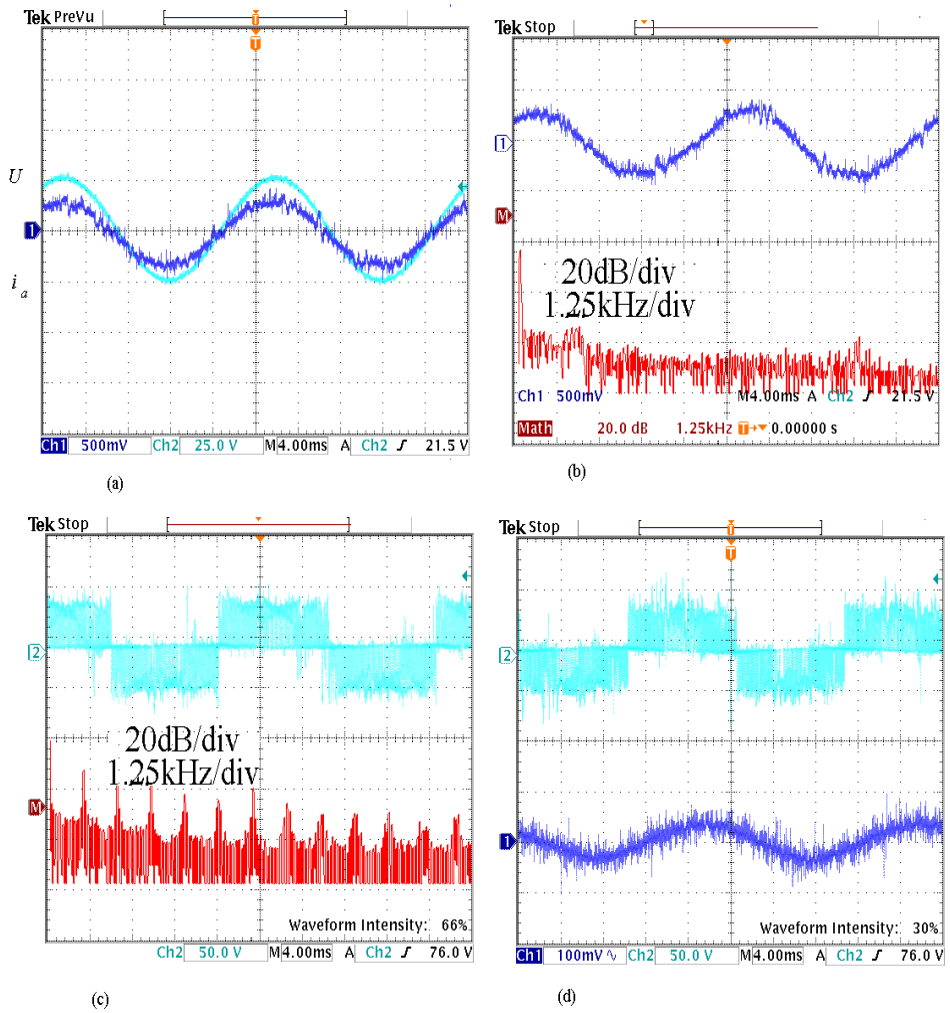

Figure 7: (a) Input phase voltage u_a and current i_a. (b) Input phase current i_a and the frequency spectrum. (c) Output line voltage and the frequency spectrum. (d) Output line voltage u_{AC} and phase current i_a.

From the frequency spectrum of Fig. 7c, it is obvious that, besides the high frequency components, the 300Hz ripple is still present in output line voltage. From Fig. 7d the novel detecting method works well, accurate current direction can be estimated, and current commutation executes reliably, even while the output current is lower.

3 Matrix converter fed induction motor drive system

3.1 Combined controller

A combined controller is proposed to implement both space vector modulation of the MC and vector control of the induction motor. Fig. 8 shows the configuration of the MC fed induction motor drive system using the combined controller. Indirect space vector modulation strategy is employed.

The direct field oriented control based on adaptive flux observer, which was applied on the PWM inverter fed induction motor drives in [10], has been used in the combined controller as the vector control strategy.

As shown in Fig. 8, the reference torque current i_t^* and reference exciting current i_m^* are determined by carrying out PI control to the motor speed error and rotor flux error, respectively. After applying PI control to the errors of torque current and exciting current, the reference voltages in d-q stationary frame V_{ds}^* and V_{qs}^* are obtained by use of vector rotation from the reference voltages in m-t synchronous rotating frame V_m^* and V_t^*:

$$\begin{cases} V_{ds}^* = V_m^* \cos\hat{\theta} - V_t^* \sin\hat{\theta} \\ V_{qs}^* = V_m^* \sin\hat{\theta} + V_t^* \cos\hat{\theta} \end{cases} \tag{7}$$

where $\hat{\theta}$ is the rotor flux angle. The estimated rotor flux and its angle are calculated by the adaptive flux observer from the stator voltage V_s and stator current i_s using discrete approximation.

$$\cos\hat{\theta} = \hat{\phi}_{dr} \Big/ \hat{\phi}_r, \quad \sin\hat{\theta} = \hat{\phi}_{qr} \Big/ \hat{\phi}_r, \tag{8}$$

$$\hat{\phi}_r = \sqrt{\hat{\phi}_{dr}^2 + \hat{\phi}_{qr}^2}. \tag{9}$$

The adaptive flux observer is given by the equations [9].

$$\dot{\hat{x}} = A\hat{x} + BV_s + G\left(\hat{i}_s - i_s\right) \tag{10}$$

where

$$x = \begin{bmatrix} i_s & \phi_r \end{bmatrix}^T,$$

$\phi_r = \begin{bmatrix} \phi_{dr} & \phi_{qr} \end{bmatrix}^T$: d-axis and q-axis rotor flux,
$V_s = \begin{bmatrix} V_{ds} & V_{qs} \end{bmatrix}^T$: d-axis and q-axis stator voltage,
$i_s = \begin{bmatrix} i_{ds} & i_{qs} \end{bmatrix}^T$: d-axis and q-axis stator current,

$$A = \begin{bmatrix} A_{11} & A_{12} \\ A_{21} & A_{22} \end{bmatrix}, \quad B = \begin{bmatrix} B_1 \\ 0 \end{bmatrix},$$

$$A_{11} = -\left\{R_s/(\sigma L_s) + (1-\sigma)/(\sigma\tau_r)\right\} I = a_{r11} J,$$

$$A_{12} = M/(\sigma L_s L_r)\left\{(1/\tau_r)\, I - \omega_r J\right\} = a_{r12} I + a_{i12} J,$$

$$A_{21} = (M/\tau_r)\, I = a_{r21} I,$$

$$A_{22} = -(1/\tau_r)\, I + \omega_r J = a_{r22} I + a_{i22} J,$$

$$B_1 = 1/(\sigma L_s) I = b_1 I, \quad \sigma_r = 1 - M^2/(L_s L_r), \quad \tau_r = L_r/R_r,$$

$$I = \begin{bmatrix} 1 & 0 \\ 0 & 1 \end{bmatrix}, \quad J = \begin{bmatrix} 0 & -1 \\ 1 & 0 \end{bmatrix},$$

R_s, R_r : stator and rotor resistance,
L_s, L_r : stator and rotor self-inductance,
M : mutual inductance,
ω_r : motor angular velocity,
G : flux observer gain.

Due to the inherent relationship between the direct field oriented control and the space vector modulation, the two strategies can be combined conveniently. From Fig. 6, it can be seen that the reference output line voltage space vector $\vec{V}_o^*$ can be directly synthesized by the reference voltages V_{ds}^* and V_{qs}^* generated from direct oriented control. As shown in Fig. 6, the modulation index m (the same as the voltage modulation index m_v), which represents the amplitude of $\vec{V}_o^*$, is obtained by

$$m = \sqrt{\left(V_{ds}^*\right)^2 + \left(V_{qs}^*\right)^2} \Big/ V_{s\,\mathrm{lim}} \ , \quad 0 \le m \le 1 \tag{11}$$

where $V_{s\,\mathrm{lim}}$ is the amplitude limitation of V_s. S_{vo}, θ_{sv}, which represent the phase angle of $\vec{V}_o^*$, can also be calculated by V_{ds}^* and V_{qs}^* based on the triangle theory. S_{ci}, θ_{cv}, which represent the phase angle of reference input phase current space vector $\vec{I}_i^*$, are determined by detected input phase voltage space vector $\vec{V}_i$ and input displacement angle φ_i. According to these variables, the combined controller calculates switching duration of space vectors, and outputs them as PWM signals to switch commutation controller, which is in charge of the commutation process of bi-directional switches.

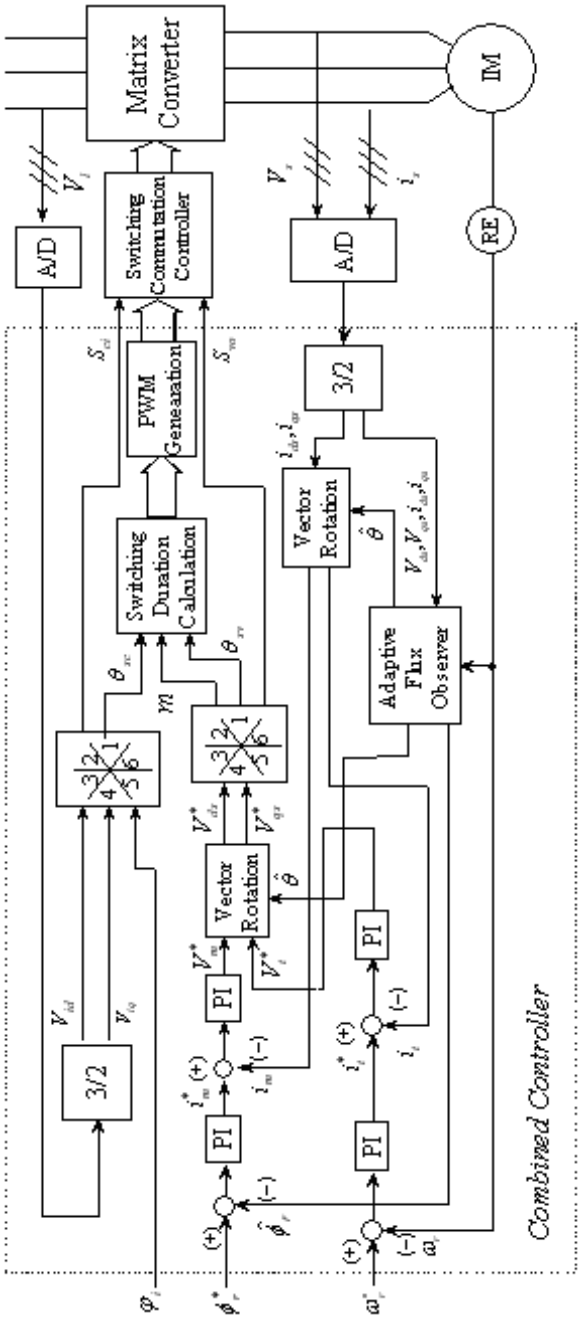

Figure 8: Combined controller for matrix converter fed induction motor drive system.

3.2 Drive performance analysis

In order to analyze the drive performance of the proposed controller, a numerical simulation of the whole system has been carried out. The MC is used to drive a standard 3.7kW four-pole 200V 62.3Hz cage induction motor having the following parameters:

$$R_s{=}0.3578\Omega,\ R_r{=}0.2861\Omega,\ L_s{=}0.03972\text{H},\ L_r{=}0.03972\text{H},\ M{=}0.03841\text{H}.$$

The simulations have been carried out assuming a sampling period of 500μs and ideal switching devices.

The dynamic behavior of the proposed controller has been tested with reference to a speed step change response and impact load response. Fig. 9 shows the increase and decrease 60r/min speed step change response at operation speed 800r/min. The impact load response is shown in Fig. 10 (load torque change: $25\%T_N \rightarrow 75\%T_N \rightarrow 25\%T_N$, rating load torque $T_N = 9.8$ Nm).

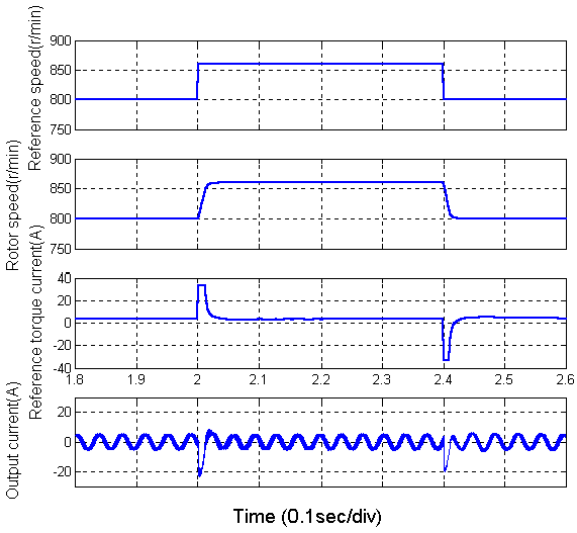

Figure 9: Speed step change response.

In both cases, the drive system exhibits a superior dynamic performance. The reference torque current rapidly changes according to the speed command and load torque, and the rotor speed stabilizes at the reference speed quickly without any vibration. During the operation, the current waveform

of the MC is almost sinusoidal immediately after the speed step command and load torque changes.

The direct bi-directional power flow capability is one of the advantages of the MC. During regeneration, most of the inertial energy is directly returned to the power grid. Thus, in all four quadrants, high energy-efficiency and very rapid speed response can be achieved [11].

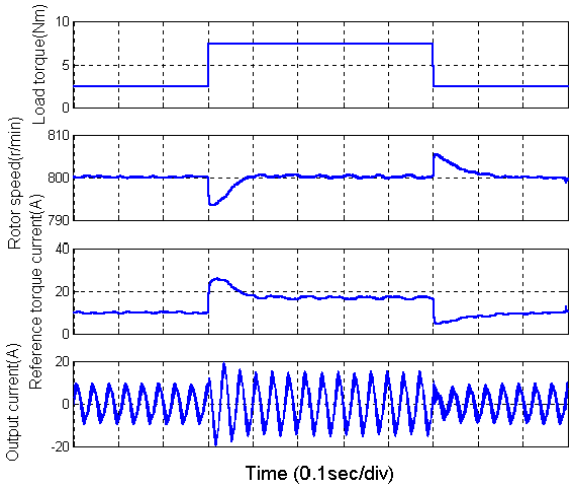

Figure 10: Impact load response.

3.3 Experimental results

In order to verify the proposed combined control strategy, a 2.7kVA experimental prototype of the MC fed induction motor drive system has been implemented. The block diagram of the prototype is shown in Fig. 11.

The LC filter is the same as the one shown in Fig. 5. The power stage of MC is realized by use of 18 600-V 30-A insulated gate bipolar transistors (IGBT's) and 18 fast-recovery diodes to make 9 bi-directional switches. A 2.2kW 380V 50Hz cage induction motor is fed by the MC in this drive system.

Experimental tests have been carried out in steady-state operation conditions on the prototype. During the operation, the reference speed is fixed at 666 r/min without a load.

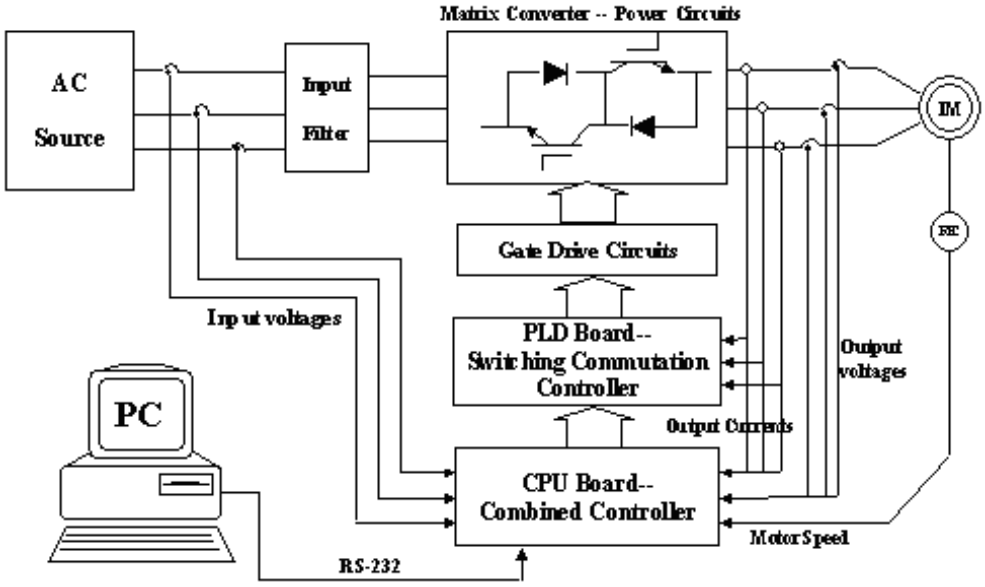

Figure 11: Block diagram of experimental prototype.

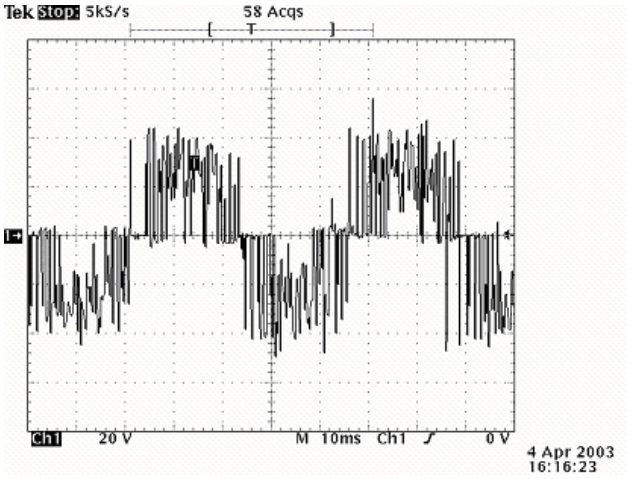

Figure 12: Output line voltage at 666r/min (20V/div, 10ms/div).

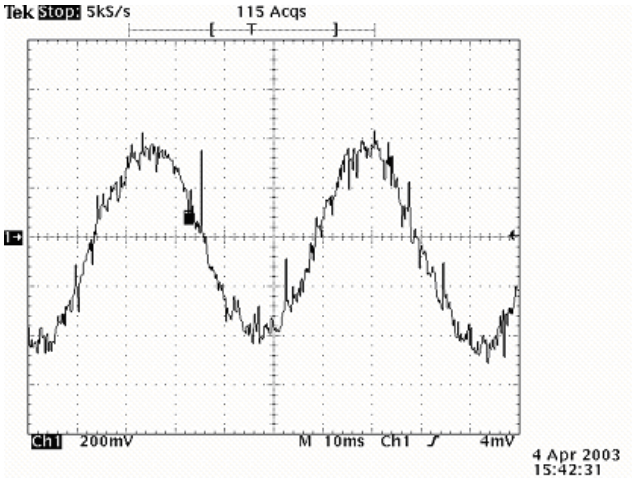

Figure 13: Output line current at 666r/min (1A/div, 10ms/div).

Figs. 12 and 13 show, respectively, the output line voltage and line current of the MC. As can be seen, the output line voltage waveform is similar to the output of convention PWM inverters, and the output line current is almost sinusoidal, confirming good behavior of the control strategy.

4 A feed-forward compensation method under abnormal input voltage conditions

4.1 Analysis of MC operation under abnormal conditions

The indirect modulation technique is employed as the control strategy of the MC, as shown in Fig. 3. Under normal conditions, the input three phase voltages can be expressed as

$$V_{iPh} = \begin{bmatrix} V_a \\ V_b \\ V_c \end{bmatrix} = V_{im} \cdot \begin{bmatrix} \cos(\omega_i t) \\ \cos(\omega_i t - 120^\circ) \\ \cos(\omega_i t + 120^\circ) \end{bmatrix} \tag{12}$$

where V_{im} is the amplitude of input phase voltage, ω_i is the input angular frequency.

Because the switching frequency of the MC system is much higher than the frequencies of the input voltages and output currents, the average output line voltages and average input phase currents can be described as sinusoidal with PWM algorithms.

The average output line voltages are given by

$$\overline{V}_{oL} = \sqrt{3} \cdot V_{om} \cdot \begin{bmatrix} \cos(\omega_o t - \varphi_o + 30^\circ) \\ \cos(\omega_o t - \varphi_o + 30^\circ - 120^\circ) \\ \cos(\omega_o t - \varphi_o + 30^\circ + 120^\circ) \end{bmatrix} \tag{13}$$

where V_{om} is the amplitude of output phase voltage, ω_o is the output angular frequency, and the φ_o is output displacement angle.

Then the input-phase to output-line transfer function matrix given by low frequency $\overline{T}_{PhL}$ should be chosen as

$$\overline{T}_{PhL} = m \cdot \begin{bmatrix} \cos(\omega_o t - \varphi_o + 30^\circ) \\ \cos(\omega_o t - \varphi_o + 30^\circ - 120^\circ) \\ \cos(\omega_o t - \varphi_o + 30^\circ + 120^\circ) \end{bmatrix} \cdot \begin{bmatrix} \cos(\omega_i t - \varphi_i) \\ \cos(\omega_i t - \varphi_i - 120^\circ) \\ \cos(\omega_i t - \varphi_i + 120^\circ) \end{bmatrix}^T \tag{14}$$

where $0 \leq m \leq 1$ is the modulation index and φ_i is an arbitrary angle [12].

The abnormal input voltage conditions usually include: unbalanced input voltages, non-sinusoidal input voltages, and short time input voltage sag. Obviously, while any condition is presented, the input voltages change and the distortion of output voltages is caused, which produces distorted output currents.

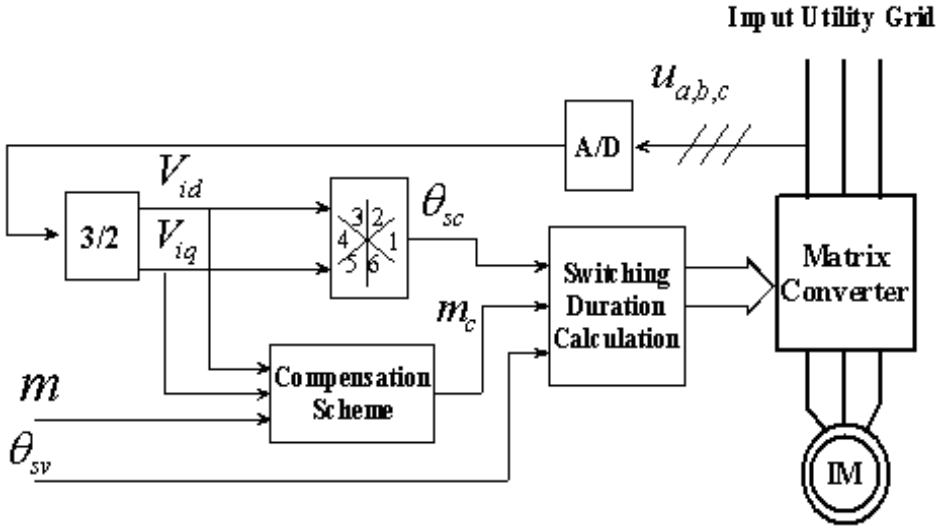

Figure 14: Feed-forward compensation method.

4.2 A feed-forward compensation method

A feed-forward compensation method based on measuring input voltages, is proposed (shown in Fig. 14). The instantaneous values of three phase input voltages are detected and transformed into d-q reference frame – V_{id} and V_{iq}. The modulation index m generated by vector control can be adjusted through a compensation scheme according to V_{id} and V_{iq} when the input voltages are unbalanced or sagged. The compensation scheme is:

$$m_c = m \cdot \left(\frac{V_{i\_ref}}{\sqrt{V_{id}^2 + V_{iq}^2}} \right) \tag{15}$$

where m_c is the compensated modulation index, V_{i_ref} is the reference magnitude of input voltage space vector under normal conditions [13].

4.3 Experimental results

A 2.7kW prototype of the MC fed induction motor drive system is implemented with the block diagram of experimental setup being the same as in the previous part (shown in Fig. 11).

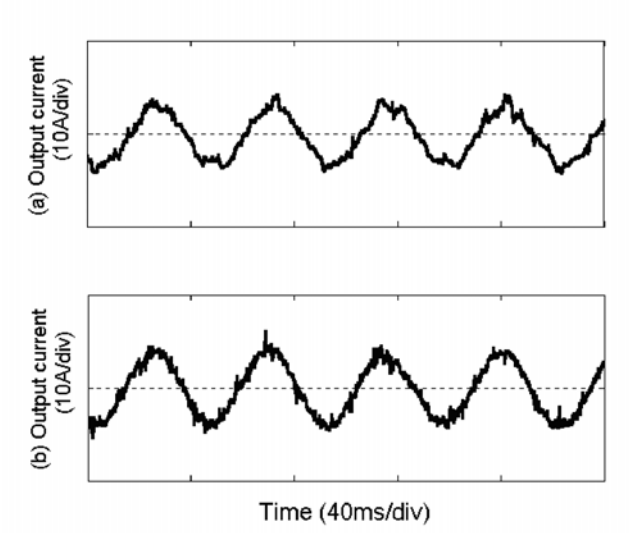

Figure 15: Output currents under input voltage unbalance: (a) without compensation; (b) with feed-forward compensation.

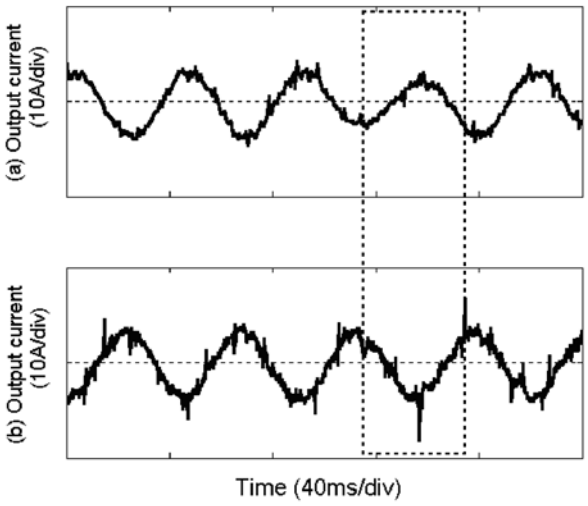

Figure 16: Output currents under input voltage sag: (a) without compensation; (b) with feed-forward compensation.

Fig. 15 shows the experimental output currents under input voltage unbalance (V_a=60V, V_b=80V, V_c=100V). Fig. 16 shows the experimental output currents with a 40ms input voltage sag (70% of rated values). From the experimental results, it can be concluded that the current waveforms are improved by the proposed compensation method. During the input voltage sag, this method works well with a fast dynamic response.

5 Conclusion

In this paper, a MC prototype is constructed by Reverse Blocking IGBTs. Accordingly, a three-stage driving method and a novel protection circuit for RB-IGBT are designed and implemented. The experimental results demonstrate that the proposed three-stage driver largely reduces the switching time and switching loss without causing the increases of turn-on di/dt and turn-off dv/dt, and different protection schemes are fulfilled respectively.

A combined controller of the MC fed induction motor drive system is proposed. This controller implements both space vector modulation of MC and direct field oriented control of induction motor. In this way, the advantages of matrix converter have been combined with the advantages of vector control technique. The proposed drive system has been tested in transient

conditions through simulations. The input/out waveforms of the MC and speed/load responses of the induction motor emphasize the effectiveness of the control scheme.

A feed-forward method to compensate the output voltages and currents of matrix converter under abnormal input voltage conditions is presented. This compensation method is simple to be implemented by measuring input voltage values, and has a very fast dynamic response. Some experimental tests demonstrate its feasibility and effectiveness.

This paper is sponsored by National Natural Science Foundation (50377014) of China and Delta Power Electronics Research & Education Foundation.

References

[1] M. Venturini, Proceedings Powercon **7**, USA, E3-1 (1980).

[2] A. Alesina and M. Venturini, IEEE Proc. PESC'88, Kyoto, Japan, 1284 (1988).

[3] L. Huber and D. Borojevic, IEEE Trans. Industry Applications **31**, 1234 (1995).

[4] S. Musumeci, A. Raciti, A. Testa, A. Galluzzo, and M. Melito, IEEE Trans. Power Electronics **12**, 645 (1997).

[5] V. John, B.S. Suh, and T.A. Lipo, IEEE Trans. Industry Applications **35**, 1108 (1999).

[6] S. Park and T.M. Jahns, Conf. Rec. IEEE-IAS Ann. Meeting, 1038 (2001).

[7] M. Takei, T. Naito, and K. Ueno, IEEE International Symposium on Power Semiconductor Devices and ICs (ISPSD), p. 156 (2003).

[8] C. Klumpner and F. Blaabjerg, Conf. Rec. IEEE-IAS Ann. Meeting, vol. **3**, p.1516 (2003).

[9] Zhichao Liu, Daning Zhou, Kai Sun, Lipei Huang, Kouki Matsuse, and Kiyoaki Sasagawa, Proc. IEEE IAS'2004, vol.**3**, p.1910, Seattle,USA (2004).

[10] H. Kubota, K. Matsuse, and T. Nakano, IEEE Trans. Industry Applications **29**, 344 (1993).

[11] Kai Sun, Lipei Huang, Kouki Matsuse, and Takashi Ishida, Proc. IAS'2003, vol. **3**, p. 1723, Salt Lake City, USA (2003).

[12] Kai Sun, Daning Zhou, Lipei Huang, and Kouki Matsuse, Proc. IEEE IAS'2004, vol.**1**, p.623, Seattle, USA (2004).

[13] Yang Mei, Kai Sun, Daning Zhou, and Lipei Huang, International Power Electronics and Motion Control Conference, IPEMC'2004, vol.**8**, p.1311 (2004).